Annalen der Physik

annalen der physik
www.ann-phys.org

RESEARCH ARTICLE OPEN ACCESS

Enhanced Electron Reflection at Mott-Insulator Interfaces

Jan Verlage | Peter Kratzer

Fakultät für Physik and CENIDE, Universität Duisburg-Essen, Duisburg, Germany

Correspondence: Jan Verlage (jan.verlage@uni-due.de)

Received: 31 January 2026 | **Revised:** 6 May 2026 | **Accepted:** 3 June 2026

Keywords: doublons/holons | hierarchy of correlations | hubbard model

ABSTRACT

The Klein paradox describes an incoming electron being scattered at a supercritical barrier to create electron–positron pairs, a phenomenon widely discussed in textbooks. While demonstrating this phenomenon experimentally with the fundamental particles remains challenging, condensed matter analogs are more accessible to experimental realization. For spinless quasi-particles, theoretical works show an enhancement of the pair production rate, and analogs of this effect in condensed matter systems have been studied theoretically. Here, another condensed matter system, a heterostructure comprised of two materials with strongly and weakly interacting electrons is presented, that allows for constructing analytical solutions using the hierarchy-of-correlations method. The results show enhanced electron reflection related with the production of doublon–holon pairs, as known from the Klein paradox.

1 | Introduction

The mathematical structure of quantum many-body physics in condensed matter physics often mirrors that of relativistic quantum theories and can thereby suggest striking analogies between otherwise distant areas of research. Such connections are particularly fruitful when equations known from relativistic physics emerge as effective descriptions of low-energy excitations in solids, enabling the parallel interpretation of results.

A prominent example of such an analogy is the Klein paradox, originally identified in the context of the Dirac equation for relativistic electrons. In his seminal work, Klein investigated the one-dimensional scattering of an electron from a potential barrier and found a finite transmission probability even when the barrier height exceeds twice the particle's rest energy and the incoming energy lies well below the barrier [1–3]. While classically forbidden, this behavior follows naturally from the relativistic wave equation and the existence of antiparticles, and has since served as a paradigmatic illustration of nontrivial quantum transport at interfaces.

Subsequent studies clarified that this effect cannot be fully understood within a single-particle framework and requires a many-body description to fully incorporate both the particle-antiparticle pair creation at sufficiently strong barriers, as well as the Pauli principle due to the presence of an incoming fermion suppressing this process [3–13]. Although these aspects are well established theoretically, direct experimental access remains challenging because of the large energy scales involved.

In contrast, condensed matter systems provide natural platforms in which analogous interface phenomena arise at much lower energies. Notably, fermionic realizations of the Klein paradox have been identified in graphene and related gapless two-dimensional materials, where chiral quasi-particles exhibit perfect transmission through potential barriers [14–17]. These observations underscore that the essential physics of the Klein paradox is not tied to fundamental particles, but rather to the structure of the underlying effective theory.

Beyond fermionic systems, bosonic analogs of the Klein paradox [6, 18–20] have also been proposed and explored in a variety of condensed matter settings [20–22]. In these systems, the absence of Pauli blocking leads to an enhancement of pair production, akin to stimulated emission, and this effect has been used as an experimental signature in platforms such as magnonic interfaces [23–25]. Importantly, the corresponding "antiparticles" are negative-energy collective excitations, avoiding the instabilities associated with fundamental bosonic antiparticles.

In this work, we introduce a correlated electronic system that provides a further solid-state realization of Klein-type interface physics. We study the interface between weakly and strongly correlated materials and demonstrate that it supports an effective description in terms of doublons and holons in a Mott insulator. These composite quasi-particles play the role of particles and antiparticles, respectively, while remaining intrinsic excitations of the lattice system and thus free of fundamental instabilities.

Unlike earlier analog realizations in optical lattices [26–37], in semiconductors [38–40] or ^{3}He [41], the effective gap in our system arises naturally from electronic correlations in the Fermi–Hubbard model, without the need for external fine-tuning. Moreover, the emergent doublon–holon symmetry closely mirrors the structure of relativistic particle and antiparticle bands, and the resulting low-energy equations of motion take a form directly analogous to a 1+1 dimensional Dirac equation. Previous work has established this analogy for specific magnetic backgrounds in the Mott phase [42], where the lower and upper Hubbard bands correspond to filled and empty continua, respectively [43–45]. Here, we go beyond these settings by addressing the role of interfaces and scattering.

The central question we address is whether reflection and transmission at a correlated interface can carry observable signatures of doublon–holon pair production in the Mott phase. By formulating the problem in terms of quasi-particle scattering, we show that the interface provides direct access to correlation-induced pair creation phenomena in a purely condensed matter context.

This paper is organized as follows. We first introduce the hierarchy of correlations used to derive the effective propagation equations for the quasiparticles. We then analyze scattering at a single interface and compute the corresponding transmission and reflection coefficients. Finally, we recast the resulting equations in a Dirac-like form to make the underlying structure transparent and to place the condensed matter results in a broader theoretical context.

2 | Hubbard Model and Hierarchy of Correlations

In order to describe both the weakly interacting layer as well as the strongly interacting Mott insulator, we employ the Hubbard model [46], defined as follows:

$$\hat{H} = -\frac{1}{Z}\sum_{\mu\nu s} t_{\mu\nu}\hat{c}^{\dagger}_{\mu s}\hat{c}_{\nu s} + \sum_{\mu} U_{\mu}\hat{n}_{\mu\uparrow}\hat{n}_{\mu\downarrow} + \sum_{\mu s} V_{\mu}\hat{n}_{\mu s}. \tag{1}$$

Here, $c^{\dagger}_{\mu s}$ and $c_{\nu s}$ denote fermionic creation and annihilation operators acting on lattice sites denoted by vectorial indices $\boldsymbol{\mu}$ and $\boldsymbol{\nu}$, respectively, with spin index $s \in \{\uparrow, \downarrow\}$. The corresponding number operators are given by $\hat{n}_{\mu s} = c^{\dagger}_{\mu s}c_{\mu s}$. The lattice structure and associated hopping amplitudes are encoded in the adjacency matrix $t_{\mu\nu}$, which is taken to be nonzero only for nearest-neighbor pairs, where it assumes the value t; otherwise, $t_{\mu\nu} = 0$. The coordination number Z counts the number of nearest neighbors per site.

The parameter U_{μ} describes the Coulomb interacting, and is only non-zero in the Mott insulator. It is worth noting that in weakly correlated semiconductors, a small on-site interaction U_{μ} may be treated within a mean-field framework and effectively absorbed into a renormalized V_{μ}, akin to the treatment in Fermi liquid theory [47, 48].

The on-site potential is, in principle, non-zero in both the strongly and weakly interacting layer, as the Mott bands are not necessarily centered around $U/2$, but might be shifted up- or downwards. In the following, we will fix the occupation numbers in the Mott insulator, which also fixes the chemical potential to zero for the Mott insulator. This chemical potential is implicitly included in the on-site potential term in the Hamiltonian. In the weakly interacting half-space, the on-site potential can formally be seen as incorporating the chemical potential; it takes a homogeneous value $V > 0$. Therefore we take $V_{\mu\in\text{Mott}} \equiv 0$ and deal with the band alignment only by $V_{\mu\in\text{semi}}$. This yields a system Hamiltonian

$$\hat{H} = -\frac{t}{Z}\sum_{\mu s} \hat{c}_{s\mu}\hat{c}_{s\mu\pm1} + \sum_{\mu\in\text{Mott}} U_{\mu}\hat{n}_{\mu\uparrow}\hat{n}_{\mu\downarrow} + \sum_{\mu\in\text{semi},s} V_{\mu}\hat{n}_{\mu s}. \tag{2}$$

In this, $\sum_{\mu s}\hat{c}s_{\mu}c_{\mu\pm1}$ denotes hopping to all possible neighboring sites. For a one-dimensional system this sum consists of two terms, for a two-dimensional square lattice of four, and so on. For the ease of notation, we use the parameters U_{μ} and V_{μ} to distinguish between strongly correlated layers ($U_{\mu} \neq 0, V_{\mu} = 0$) and weakly correlated layers ($U_{\mu} = 0, V_{\mu} \neq 0$) within the system under investigation, although more general choices of parameters are physically meaningful as well.

2.1 | Hierarchy of Correlations

To approximate solutions for charge modes at the interface, we employ the hierarchy of correlations [49–52], which is particularly well-suited for systems with a large coordination number $Z \gg 1$. In this framework, reduced density matrices involving two or more lattice sites are decomposed into on-site and correlated components. Specifically, for a pair of lattice sites $\boldsymbol{\mu}$ and $\boldsymbol{\nu}$, this decomposition reads $\hat{\rho}_{\mu\nu} = \hat{\rho}_{\mu}\hat{\rho}_{\nu} + \hat{\rho}^{\text{corr}}_{\mu\nu}$. Based on the assumption $Z \gg 1$, one can perform an expansion in powers of $1/Z$, leading to a natural suppression of higher-order correlators. The two-point correlation scales as $\hat{\rho}^{\text{corr}}_{\mu\nu} = \mathcal{O}(Z^{-1})$, while the three-point correlation satisfies $\hat{\rho}^{\text{corr}}_{\mu\nu\lambda} = \mathcal{O}(Z^{-2})$, and so on.

Performing this expansion into the inverse coordination number, the evolution equations form an infinite hierarchy. Here, we exhibit only the first two, which are the ones we actually use for our further calculations, they read

$$\begin{aligned} i\partial_t\hat{\rho}_{\mu} &= F_1(\hat{\rho}_{\mu}, \hat{\rho}^{\text{corr}}_{\mu\nu}), \\ i\partial_t\hat{\rho}^{\text{corr}}_{\mu\nu} &= F_2(\hat{\rho}_{\mu}, \hat{\rho}^{\text{corr}}_{\mu\nu}, \hat{\rho}^{\text{corr}}_{\mu\nu\lambda}). \end{aligned} \tag{3}$$

TABLE 1 | Group velocity of the Mott–Néel solutions inside the bands.

	lower Hubbard band	**upper Hubbard band.**
$v_G(\kappa_1)$	< 0	> 0
$v_G(\kappa_3)$	> 0	< 0

The exact form of the functionals F_n depends on the specific structure of the Hamiltonian. By using the fact that $\hat{\rho}^{\mathrm{corr}}_{\mu\nu} = \mathcal{O}(Z^{-1})$ we approximate this to:

$$\begin{aligned} i\partial_t \hat{\rho}_\mu &\approx F_1(\hat{\rho}_\mu, 0), \quad \text{with solution } \hat{\rho}^0_\mu, \\ i\partial_t \hat{\rho}^{\mathrm{corr}}_{\mu\nu} &\approx F_2(\hat{\rho}^0_\mu, \hat{\rho}^{\mathrm{corr}}_{\mu\nu}, 0). \end{aligned} \tag{4}$$

This hierarchy yields an iterative scheme for approximating the full density operator $\hat{\rho}$. Further details of the method are provided in Appendix A.

In analogy with the Hubbard X operators [53, 54] and composite operator methods [55], we introduce quasi-particle operators defined as:

$$\hat{c}_{\mu s I} = \hat{c}_{\mu s}\hat{n}^I_{\mu\bar{s}} = \begin{cases} \hat{c}_{\mu s}(1 - \hat{n}_{\mu\bar{s}}), & \text{for } I = 0, \\ \hat{c}_{\mu s}\hat{n}_{\mu\bar{s}}, & \text{for } I = 1, \end{cases} \tag{5}$$

where $I = 1$ corresponds to doublons and $I = 0$ to holons. These are the physical excitations within the Mott insulator on top of the half-filled background. From these operators, we define the corresponding correlation functions $\langle \hat{c}_{\mu s I}\hat{c}_{\nu s J}\rangle^{\mathrm{corr}}$ [56].

2.2 | Factorization

For the relevant dynamics, these correlators may be factorized [49, 57] as:

$$\langle \hat{c}_{\mu s I}\hat{c}_{\nu s J}\rangle^{\mathrm{corr}} = (p^I_{\mu s})^* p^J_{\nu s}, \tag{6}$$

where $p^1_{\mu s}$ and $p^0_{\mu s}$ are the doublon and holon amplitudes, respectively. These amplitudes can be combined into a spinor representation, from which the equations of motion for the (quasi-)particles can be derived [56]. In a sense, this is the same as factorizing the many-body density operator $\hat{\rho}$ in this doublon–holon basis as $\hat{\rho}_{IJ} = \left(p^I\right)^* p^J$ with the wave functions p^I.

In the interface system, the translational invariance is broken in only one direction, in the other ones it is still intact. Therefore, we can decompose the quasi-particle wave functions into their parallel momentum $k^{\parallel}$ dependent Fourier components. After this, the index μ is just a scalar counting the layers parallel to the interface. In a hyper-cubic lattice the Schrödinger-like equations for doublons $I = 1$ and holons $I = 0$ can be combined

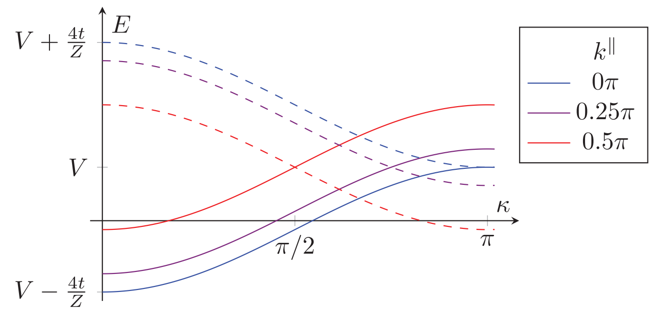

FIGURE 1 | Energy bands as a function of momentum κ for different parallel momenta $k^{\parallel}$ for the even (solid lines) and odd (dashed lines) spinor solution in the weakly interacting layers.

using $U^I_\mu = IU_\mu$:

$$\begin{aligned} \left(E - U^I_\mu - V_\mu\right)p^I_{\mu s} + \langle \hat{n}^I_{\mu\bar{s}}\rangle^0 \sum_J t^{\parallel}_{\mathbf{k}} p^J_{\mu s} \\ = -t\frac{\langle \hat{n}^I_{\mu\bar{s}}\rangle^0}{Z} \sum_J \left(p^J_{\mu-1\,s} + p^J_{\mu+1\,s}\right). \end{aligned} \tag{7}$$

The expectation values $\langle \hat{n}^I_\mu\rangle^0$ are evaluated with respect to the mean-field background state $\hat{\rho}^0_\mu$. $t^{\parallel}_{\mathbf{k}} = 2t/Z\sum_i \cos(k^{\parallel}_i)$ is the kinetic energy contribution from the bands formed in the translational invariant directions for nearest neighbor hopping. For hyper-cubic lattice this means $Z = 4$ in two dimensions and $Z = 6$ in three dimensions. Moreover, this choice is not just guided by mathematical simplicity, but also by pervoskite structures in which the essential Mott physics happens on a cubic lattice and heterostructures from these material class can be grown with high precision. A detailed derivation of this equation is provided in Appendix B or [56]. For more details about interface systems within the hierarchy see, for example, [52, 56]. Obviously, the effective coordination number of sites at the interface can generally be different from bulk, depending on the local topology. In the case chosen here with same hopping parameters in both half-spaces and the interface coinciding with a lattice plane, the effective coordination does not change. In other cases, for example with different hopping in the two half-spaces, this is not true anymore. By design, the hierarchy always describes the strongly correlated physics for non-zero U, such that local changes to the effective coordination number result in only quantitative, but not in qualitative changes [52].

To first order, the two spin sectors decouple. Because of this, we will work from now on in the spin $\uparrow$ sector and drop the index s. In our expansion, the dynamics of the spin fluctuations is suppressed by an additional order $1/Z$, such that we treat the charge modes dynamic as it happens on top of a fixed spin background.

2.3 | Mott-Neel Type Spin Order

The starting point of our analysis is the mean-field background. It is needed to analyze the effective Equation (7). The Mott insulator state has one particle per site, it is half-filled. This leaves the spin degree of freedom. In this work, we consider

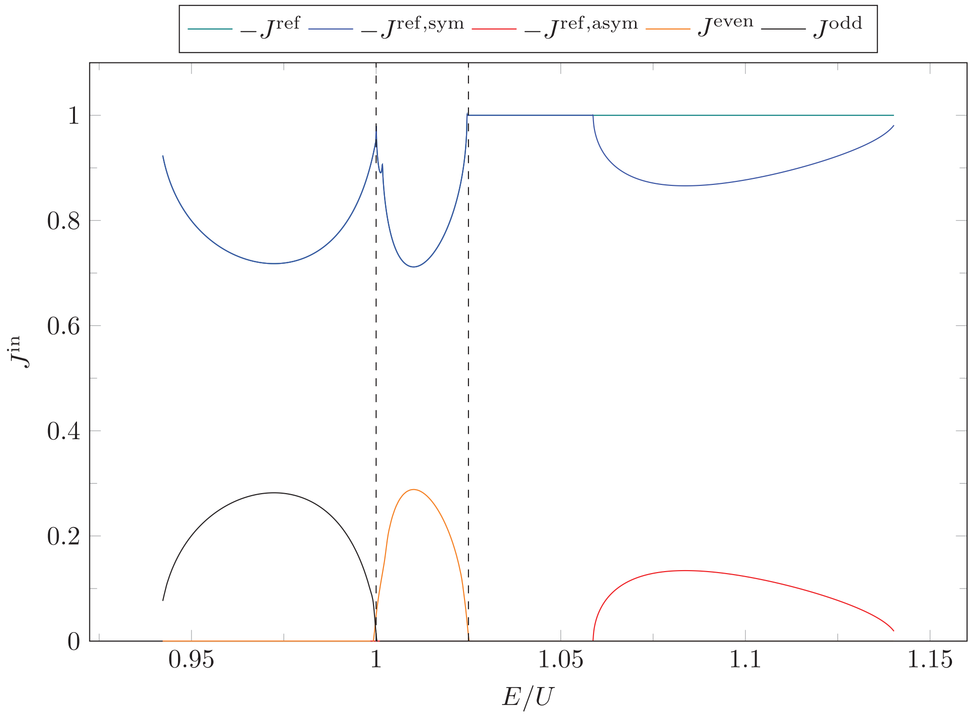

FIGURE 2 | Reflected and transmitted currents as function of energy in a two-dimensional lattice with $V = 1.1U$, $t = 0.2U$, $Z = 4$ and $k^{\parallel} = 0.3\pi$ for energies greater than half the bandgap, $E > U/2$. Dashed vertical lines mark the edges of the upper Hubbard band. At $E/U \approx 1.6$ the asymmetric current $J^{\text{ref,asym}}$ becomes non-zero. For this energy, there is a band overlap between the symmetric and antisymmetric spinor solution within the weakly interacting half-space. The "kink" around $E/U \approx 1$ is an artifact of the numerical resolution.

the antiferromagnetic Mott–Néel state with its checkerboard structure:

$$\hat{\rho}^0_\mu = \begin{cases} |\uparrow\rangle\langle\uparrow| & \mu \in A, \\ |\downarrow\rangle\langle\downarrow| & \mu \in B. \end{cases} \tag{8}$$

Because of the sublattice structure, an additional index A and B is necessary. The expectation values are fixed as $\langle \hat{n}_{\mu_A \uparrow}\rangle = 1, \langle \hat{n}_{\mu_B \uparrow}\rangle = 0$. The weakly interacting layer coupled to this will inherit the bipartite structure. For this, we take either the valence band $|\uparrow\downarrow\rangle$ or the conduction band $|0\rangle$. Because our calculation is done at zero temperature, these two are related via the particle-hole symmetry.

From the spin ordering of the background, it follows directly that:

$$E\, p^{1_A}_\mu = (E - U)\, p^{0_B}_\mu \equiv 0. \tag{9}$$

Hence, in the Mott–Néel state the coupled equations for doublons and holons thus read:

$$\begin{aligned} E p^{0_A}_\mu &= -\left[t^{\parallel}_{\mathbf{k}} p^{1_B}_\mu + \frac{t}{Z}\left(p^{1_B}_{\mu+1} + p^{1_B}_{\mu-1} \right) \right], \\ (E-U) p^{1_B}_\mu &= -\left[t^{\parallel}_{\mathbf{k}} p^{0_A}_\mu + \frac{t}{Z}\left(p^{0_A}_{\mu+1} + p^{0_A}_{\mu-1} \right) \right]. \end{aligned} \tag{10}$$

In the weakly interacting layer, on the other hand, we find:

$$\begin{aligned} (E-V) p^{0_A}_\mu &= -\left[t^{\parallel}_{\mathbf{k}} p^{0_B}_\mu + \frac{t}{Z}\left(p^{0_B}_{\mu+1} + p^{0_B}_{\mu-1} \right) \right], \\ (E-V) p^{0_B}_\mu &= -\left[t^{\parallel}_{\mathbf{k}} p^{0_A}_\mu + \frac{t}{Z}\left(p^{0_A}_{\mu+1} + p^{0_A}_{\mu-1} \right) \right]. \end{aligned} \tag{11}$$

3 | Quasi-Particle Propagation

In order to calculate the transmission characteristics at the interface between the weakly correlated layer and the strongly correlated Mott insulator, we first need to derive the propagation within the individual regions. Otherwise we could not use the correct *ansatz* for the incoming, reflected and transmitted spinor.

3.1 | Strongly Correlated Layer

From Equation (10) we can read off that there is a proportionality between the particle $p^{1_B}_\mu$ and hole $p^{0_A}_\mu$ solution on their respective sublattices, they are not independent. Thus, in the *ansatz* $p^{1_B}_\mu = \mathcal{B}\kappa^\mu$ and $p^{0_A}_\mu = \mathcal{A}\kappa^\mu$ the amplitudes $\mathcal{A}$ of the holons and $\mathcal{B}$ of the doublon wave functions are related. Their relative sign allows us to distinguish two cases, $p^{1_B}_\mu = \beta p^{0_A}_\mu$ with $\beta = \pm\sqrt{\frac{E}{E-U}}$. The one with the plus is called the even spinor, the other one the odd spinor. The odd one has a phase shift from one sublattice to the other.

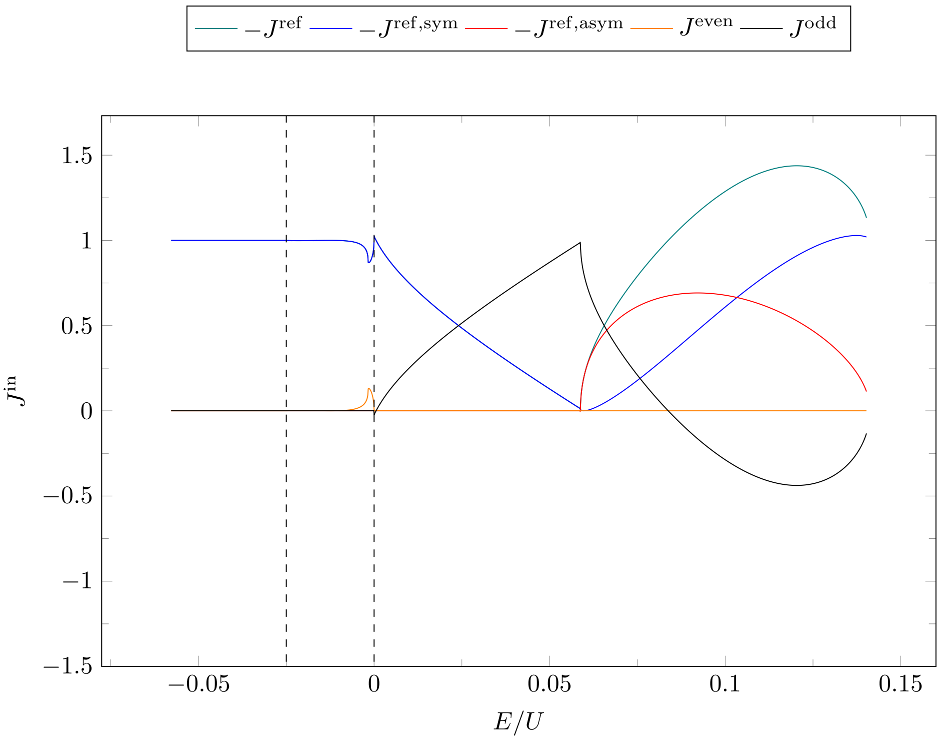

(a) Contribution to the current in single interface for $V = 0.1U$. Dashed lines delineate the energy interval of the lower Hubbard band. For an energy of $E/U \approx 0.06$ the asymmetric reflected current $J^{\mathrm{ref,asym}}$ becomes non-zero. At this energy, the band overlap in the weakly interacting layer starts to appear, and subsequently the reflection rises above 1. For an energy slightly below zero, there is a "kink" in the reflection due to transmission via the even current J^{even} in the lower Hubbard band.

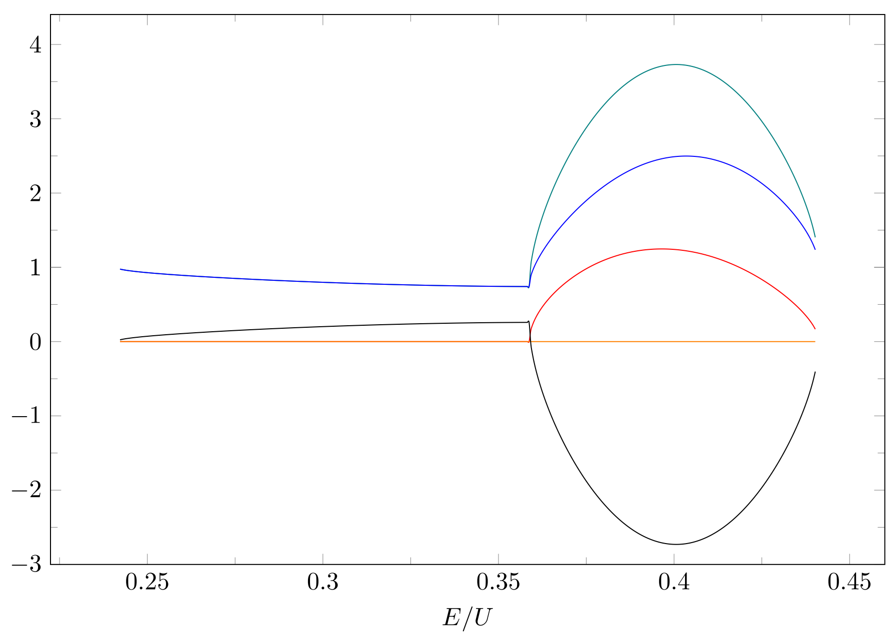

(b) Same as (a) for $V = 0.4U$. For an energy of $E/U \approx 0.36$ the asymmetric reflected current $J^{\mathrm{ref,asym}}$ becomes non-zero. At this energy, the band overlap in the weakly interacting layer starts to appear, and subsequently the reflection rises above 1.

FIGURE 3 | Reflected and transmitted currents in units of the incoming one as function of energy in a two-dimensional lattice with $t = 0.2U$, $Z = 4$ and $k^{\parallel} = 0.3\pi$ for energies smaller than half the bandgap, $E < U/2$.

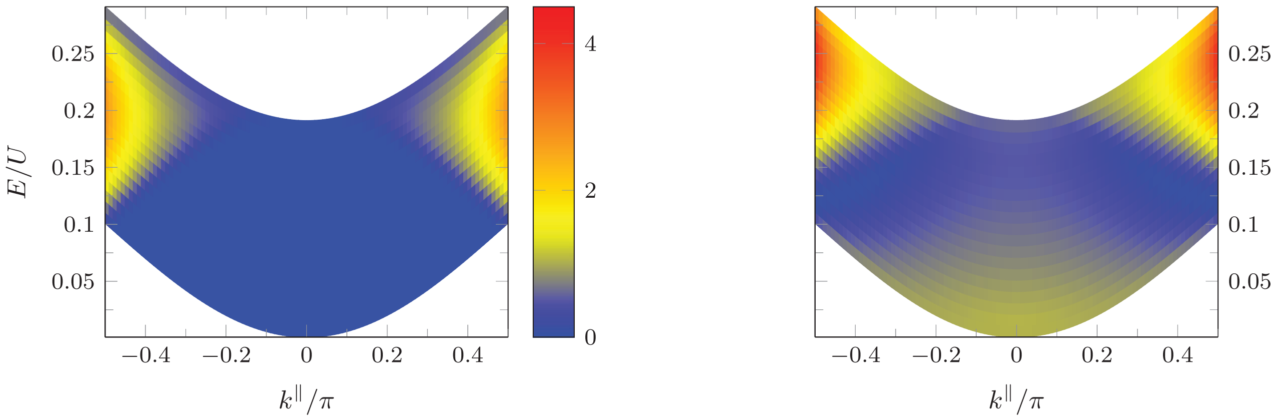

(a) $-J^{\mathrm{refl,asym}}$ **(b)** $-J^{\mathrm{refl,sym}}$

FIGURE 4 | Density plot of the reflected current for the (a) asymmetric and (b) symmetric reflection as a function of parallel momentum and energy. The plots use the same color scaling, the parameters are $V = 0.2U$, $t = 0.2U$ in a two-dimensional lattice.

We find the eigenmodes:

$$\begin{aligned}\kappa_{1,2} &= -\frac{Z}{2t}\left(\sqrt{E(E-U)} + t_{\mathbf{k}}^{\parallel}\right)\\ &\quad\pm\sqrt{\left[\frac{Z}{2t}\left(\sqrt{E(E-U)} + t_{\mathbf{k}}^{\parallel}\right)\right]^2 - 1},\\ \kappa_{3,4} &= +\frac{Z}{2t}\left(\sqrt{E(E-U)} - t_{\mathbf{k}}^{\parallel}\right)\\ &\quad\pm\sqrt{\left[\frac{Z}{2t}\left(\sqrt{E(E-U)} - t_{\mathbf{k}}^{\parallel}\right)\right]^2 - 1}\end{aligned} \tag{12}$$

with $\kappa_1\kappa_2 = \kappa_3\kappa_4 = 1$. Within the Hubbard bands, they are complex numbers obeying $|\kappa_i| = 1$, such that $p_\mu^{1_B}$ and $p_\mu^{0_A}$ describe plane waves. This can be seen by applying the identity $x \pm i\sqrt{1-x^2} = e^{\pm i\arccos(x)}$, which defines the effective wave numbers for the propagation. They read:

$$\begin{aligned}\cos(x_{1,2}) &= \frac{Z}{2t}\left(\sqrt{E(E-U)} + t_{\mathbf{k}}^{\parallel}\right)\\ \cos(x_{3,4}) &= \frac{Z}{2t}\left(\sqrt{E(E-U)} - t_{\mathbf{k}}^{\parallel}\right).\end{aligned} \tag{13}$$

The proportionality between them reads:

$$\mathcal{B}_i = \frac{1}{U-E}\left[t_{\mathbf{k}}^{\parallel} + \frac{t}{Z}\left(\kappa_i + \kappa_i^{-1}\right)\right]\mathcal{A}_i, \tag{14}$$

which yields the β with the correct sign. κ_1 and κ_2 belong to the even solutions, i.e. having the same sign on neighboring sites of both sublattices, while κ_3 and κ_4 belong to the odd solutions with a sign change between sublattices. The propagation direction of the individual modes is dictated by the group velocity:

$$v_G(\kappa_i) = -i\frac{1}{\kappa_i}\frac{\mathrm{d}\kappa_i}{\mathrm{d}E}, \tag{15}$$

which reads for the four modes

$$\begin{aligned}v_G(\kappa_1) = -v_G(\kappa_2) &= \frac{Z}{8t}\frac{2E-U}{\sqrt{E(E-U)}}\\ &\quad\frac{1}{\sqrt{1-\left[\frac{Z}{2t}\left(\sqrt{E(E-U)} + t_{\mathbf{k}}^{\parallel}\right)\right]^2}},\\ v_G(\kappa_3) = -v_G(\kappa_4) &= -\frac{Z}{8t}\frac{2E-U}{\sqrt{E(E-U)}}\\ &\quad\frac{1}{\sqrt{1-\left[\frac{Z}{2t}\left(\sqrt{E(E-U)} - t_{\mathbf{k}}^{\parallel}\right)\right]^2}}\quad.\end{aligned} \tag{16}$$

There is a sign change in the middle of the Mott gap $U/2$. For the lower energies, κ_2 and κ_3 describe right-propagating solutions, for higher ones κ_1 and κ_4 do this, see Table 1. This is relevant to find the correct *ansatz* for the transmitted spinor. Inside the Mott bands the group velocity is purely real, while in between the bands, $0 \le E \le U$, the group velocity turns complex. This describes both a propagation and a non-constant norm of the spinor, and already gives a first hint toward to Klein paradox analog. Outside the bands, the group velocity is purely imaginary, resulting in decaying solutions.

3.2 | Weakly Correlated Layer

In the semiconductor adjacent to the Mott insulator in the Mott–Neél state we also impose the bi-partite lattice structure, such that we can again define the checkerboard sublattices A and B. In this, the proportionality reads $p_\mu^{0_A} = \alpha p_\mu^{0_B}$. This α describes the symmetry of the hole solution $p_\mu^{0_X}$ between the two sublattices. There is an even symmetry with $p_\mu^{0_A} = p_\mu^{0_B}$ and an odd one with $p_\mu^{0_A} = -p_\mu^{0_B}$. Both of these solve Equation 11. Together with the *ansatz* λ^μ, we find the eigenmodes for $\alpha = +1$ as

$$\lambda_\pm = -\frac{Z}{2t}\left(E - V + t_{\mathbf{k}}^{\parallel}\right) \pm \sqrt{\left[\frac{Z}{2t}\left(E - V + t_{\mathbf{k}}^{\parallel}\right)\right]^2 - 1}. \tag{17}$$

This is the even solution and has a group velocity

$$v_G(\lambda_+) = -i\frac{1}{\lambda_+}\frac{\mathrm{d}\lambda_+}{\mathrm{d}E} = \frac{Z}{2t}\frac{1}{\sqrt{1-\left(\frac{Z}{2t}\left((E-V+t^{\parallel}_{\mathbf{k}})\right)^2\right)}} > 0. \tag{18}$$

λ_+ describes right-propagating solutions, λ_- left-propagating ones. The effective wave number is a solution of $\cos(k) = \frac{Z}{2t}(E - V + t^{\parallel}_{\mathbf{k}})$.

Similar for $\alpha = -1$, we find with $p^{0A}_\mu = \rho^\mu$:

$$\rho_\pm = +\frac{Z}{2t}\left(E - V - t^{\parallel}_{\mathbf{k}}\right) \pm \sqrt{\left[\frac{Z}{2t}\left(E - V - t^{\parallel}_{\mathbf{k}}\right)\right]^2 - 1}. \tag{19}$$

This is the odd solution with

$$v_G(\rho_+) = -i\frac{1}{\rho+}\frac{\mathrm{d}\rho+}{\mathrm{d}E} = -\frac{Z}{2t}\frac{1}{\sqrt{1-\left(\frac{Z}{2t}\left((E-V-t^{\parallel}_{\mathbf{k}})\right)^2\right)}} < 0. \tag{20}$$

For the odd solution $\rho_\pm$ the propagation direction is reversed. ρ_+ describes left-propagating solutions, ρ_- right-propagating ones. These are the negative energy modes related to the Klein paradox analog. The effective wave number is a solution of $\cos(k) = \frac{Z}{2t}(E - V - t^{\parallel}_{\mathbf{k}})$.

The dispersion relation $E(\kappa)$ in the weakly interacting region is shown in Figure 1 for different parallel momenta. For any non-zero parallel momentum there is a band overlap at $E = V$, allowing scattering from one band into the other.

3.3 | Probability Current

The effective (quasi-)particles in the weakly and strongly correlated half spaces are the electrons and doublons/holons, respectively. In order to physically make sense out of the transmission coefficients we need to introduce a probability current J_μ by the continuity equation:

$$\partial_t D_\mu = J_\mu - J_{\mu-1} \tag{21}$$

with the quasi-particle density:

$$D_\mu = \sum_{\ell,X} |p^{\ell X}_\mu|^2. \tag{22}$$

From the general evolution for the bi-partite lattice case Equation (7), we find the quasi-particle current as:

$$J_\mu = i\frac{t}{Z}\sum_{ilX} N^{iX}_\mu \left(p^{l\bar{X}}_{\mu+1}\left(p^{iX}_\mu\right)^* - p^{iX}_\mu\left(p^{l\bar{X}}_{\mu+1}\right)^*\right). \tag{23}$$

It is important to note that the derived quasi-particle current and subsequent derived transmission and reflection rates are not directly corresponding to measurable charge or spin current. A charge current can be calculated by introducing alternating signs of the contributions, $C_\mu = \sum_{\ell,X}(-1)^{\ell+1}|p^{\ell X}_\mu|^2$.

4 | Scattering at the Interface

We want to calculate the transmission coefficients at the interface for an incoming electron in the even spinor traveling from the weakly interacting half-space at $\mu \le 0$ onto the interface with the Mott insulator at $\mu > 0$. For this scenario, the *ansatz* in the weakly interacting space reads

$$\psi_{\mu\le 0} = \begin{bmatrix} p^{0A}_\mu \\ p^{1A}_\mu \\ p^{0B}_\mu \\ p^{1B}_\mu \end{bmatrix} = \frac{1}{2}\left(\lambda^\mu_+ + \frac{R_1}{\lambda^\mu_+}\right)\begin{bmatrix} 0 \\ 1 \\ 0 \\ 1 \end{bmatrix} + \frac{1}{2}\frac{R_2}{\rho^\mu_-}\begin{bmatrix} 0 \\ 1 \\ 0 \\ -1 \end{bmatrix}. \tag{24}$$

and in the Mott insulator

$$\psi_{\mu>0} = \frac{1}{\sqrt{2}}\frac{1}{N_i}\kappa^\mu_i\begin{bmatrix} \mathcal{A}_i \\ 0 \\ 0 \\ \mathcal{B}_i \end{bmatrix} + \frac{1}{\sqrt{2}}\frac{1}{N_j}\kappa^\mu_j\begin{bmatrix} \mathcal{A}_j \\ 0 \\ 0 \\ \mathcal{B}_j \end{bmatrix}. \tag{25}$$

The choice of κ_i and κ_j depends on the energy. Inserting this *ansatz* into Equation (23) quickly gives the incoming and reflected current:

$$\begin{aligned} j^{\mathrm{in}} &= i\frac{t}{Z}\left[\lambda_+ - \lambda^*_+\right], \\ j^{\mathrm{ref}} &= -i\frac{t}{Z}\left(|R_1|^2\left[\lambda_+ - \lambda^*_+\right] - |R_2|^2\left[\rho_- - \rho^*_-\right]\right). \end{aligned} \tag{26}$$

The incoming current is only comprised, as per *ansatz*, of the even spinor λ_+, while the reflected current comprises both the even λ_+ and the odd ρ_- with different sign.

In the strongly interacting half-space, the Mott–Néel structure fixes two components to zero. Together with $N^{0A}_\mu = N^{1B}_\mu = 1$ there is only $p^{0A}_\mu \ne 0$ and $p^{1B}_\mu \ne 0$. Therefore the current reads

$$J^{\mathrm{Mott}}_\mu = \begin{cases} i\frac{t}{Z}J^{\mathrm{even}}_\mu & \text{inside Mott bands,} \\ i\frac{t}{Z}J^{\mathrm{odd}}_\mu & 0 < E < U, \\ 0 & E < 0 \text{ or } E > U \end{cases} \tag{27}$$

with

$$\begin{aligned} 2J^{\mathrm{even}}_\mu =& \left(\tilde{A}_i\tilde{B}^*_i + \tilde{A}^*_i\tilde{B}_i\right)\left(\kappa_i - \kappa^{-1}_i\right) \\ &+ \left(\tilde{A}_j\tilde{B}^*_j + \tilde{A}^*_j\tilde{B}_j\right)\left(\kappa_j - \kappa^{-1}_j\right), \\ 2J^{\mathrm{odd}}_\mu =& \kappa^2_i\kappa^{-1}_j\left(\tilde{B}_i\tilde{A}^*_j + \tilde{A}_i\tilde{B}^*_j\right) \\ &- \kappa^{-2}_i\kappa^1_j\left(\tilde{A}_j\tilde{B}^*_i + \tilde{B}_j\tilde{A}^*_i\right) \\ &+ \kappa^2_j\kappa^{-1}_i\left(\tilde{B}_j\tilde{A}^*_i + \tilde{A}_j\tilde{B}^*_i\right) \\ &- \kappa^{-2}_j\kappa^1_i\left(\tilde{A}_i\tilde{B}^*_j + \tilde{B}_i\tilde{A}^*_j\right). \end{aligned} \tag{28}$$

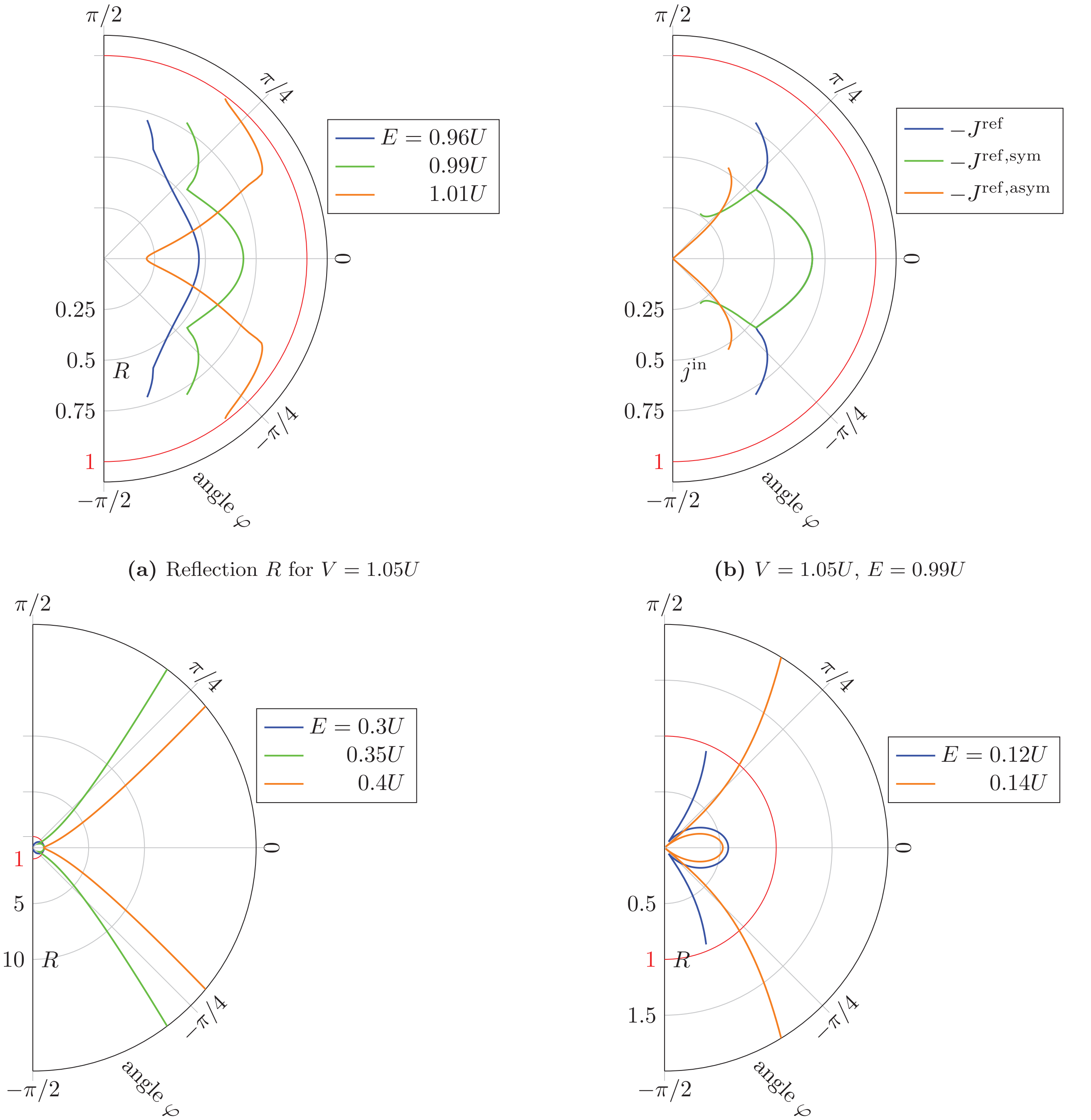

(a) Reflection R for $V = 1.05U$

(b) $V = 1.05U$, $E = 0.99U$

(c) Reflection R for $V = 0.4U$

(d) Reflection R for $V = 0.2U$

FIGURE 5 | Incident angle dependence of the reflection R and $-J^{\mathrm{ref,sym}}$, $-J^{\mathrm{ref,asym}}$ for different on-site potentials and energies. The radial axis is cropped for better visibility.

In these equations, we introduced the abbreviations $\tilde{A}_i = \mathcal{A}_i/N_i$ and $\tilde{B}_i = \mathcal{B}_i/N_i$. These quasi-particle currents are independent of the lattice site μ. From the currents we can already read off that perfect reflection only happens outside the Mott bands for $E > U$ and $E < 0$. Inside the Mott bands, there is transmission of the even current contribution, inside the gap of the odd one. For any parameter combination, independent of the energy, the conservation of the quasi-particle current

$$J^{\mathrm{even}} + J^{\mathrm{odd}} - J^{\mathrm{ref}} = J^{\mathrm{in}} \tag{29}$$

always holds. The negative sign in front of the reflected current is due to the different propagation direction.

Because of the sign change in the group velocity in the middle of the bandgap at $E = U/2$, we need to distinguish these two cases: For energies above $U/2$ – where the transmission is dominated by doublons – and below – where transmission is dominated by holons – we find different physics.

Furthermore, we will distinguish between reflection from the incoming even spinor into the even spinor, denoted as $J^{\mathrm{ref,sym}}$, and from the even into the odd one, denoted as $J^{\text{ref,asym}}$. Their sum is the total reflected current $J^{\text{ref}} = J^{\text{ref,sym}} + J^{\text{ref,asym}}$. With this, we can also define the transmission $T = J^{\text{Mott}}/J^{\text{in}}$ and reflection coefficient $R = -J^{\text{ref}}/J^{\text{in}}$, respectively. The additional minus sign compensates the different propagating directions.

For the charge current, the roles of J^{even}_μ and J^{odd}_μ are reversed. This current is lattice-site dependent and grows exponentially as e^μ for $E < U$. This is a typical issue of any stationary treatment of phenomena creating particles, also known from the usual Klein paradox.

4.1 | Regular Reflection

As a first example, we study the scattering of a particle hitting the interface from the weakly interacting half-space. For $E > U/2$, the reflected and transmitted current are plotted in Figure 2. We discuss the reflection as function of the energy E. As already expected from the band overlap in Figure 1, there is reflection from the incoming even into the odd spinor (red line). It sets on as soon as the bands energetically overlap, but remains smaller than the reflection back into the even spinor (blue line). Inside the bandgap there is transmission via the odd current combination (black line), whereas inside the upper Hubbard band the transmission happens via the even one alone (orange line). For all energies $0 \leq T \leq 1$ and $0 \leq R \leq 1$ holds. In summary, we observe the usual transmission characteristics at interfaces already known from standard quantum mechanics problems.

4.2 | Analogy to the Klein Paradox

Different behavior is encountered for $E < U/2$, as shown in Figure 3 for two choices of the on-site potential. For such energies the transmission in the Mott insulator is holon-dominated.

Generally, inside the lower Hubbard band the transmission is smaller compared to the upper one and strongly depends on the hopping strength. Larger hopping increases the transmission probability. For an energy slightly less than zero, there is a "kink" in the reflection. For this small energy range, there is a strong change in the transmission via the even current J^{even} in the lower Hubbard band, see Figure 3a. The detailed behavior depends on the band alignment.

There is still reflection into both spinors, into the even (blue line) and odd (red line) one. Different from the previous case $E > U/2$, now $R > 1$ becomes possible inside the bandgap. This is always compensated by $T < 0$ (black line), such that $R + T = 1$, to conserve the total current. Subject to an incoming electron, stimulated emission of doublon–holon pairs occurs at the interface with an amplitude given by $|T(E)|$ [20].

As the energy E is increased, there is always an initial increase of J^{odd} prior to the sign change of T from positive to negative. This is similar to the Klein paradox in graphene, that shows perfect transmission because of the chirality of the particles [14, 16], or the one for magnons at ferromagnetic interfaces, where the bosonic Klein paradox analog leads to a stimulated emission and enhances spin currents [23–25].

The amplitude of the Klein paradox increases with equalizing the amount of doublons and holons taking part in the transmission. This increases from purely holon dominated in the lower Hubbard band toward a ratio of one in the middle of the bandgap. The closer the energy is to this midpoint, the larger the amplitude, as shown in Figure 3a,b, such that the reflection from the even into the even $J^{\text{ref,sym}}$ and into the odd $J^{\text{ref,asym}}$ exceeds one. For the maximum amplitude, the symmetric reflection is always greater than the antisymmetric one. The two amplitudes are shown in Figure 4 as a function of the parallel momentum and energy as a color plot. $J^{\text{ref,sym}}$ shows the Klein paradox analog for small energies and small parallel momentum, while $J^{\text{ref,asym}}$ shows it for larger energies and large parallel momentum.

We note that we performed additional calculations with different hopping parameters inside the two half-spaces as well as for the hopping from the weakly correlated region into the strongly correlated one. The qualitative result does not change, the analog to the Klein paradox is independent of the specific hopping strengths; only the magnitude and on-set do change.

4.3 | Effective Dirac Equation

In order to understand the origin of the Klein paradox analog in this condensed matter system we will derive an effective Dirac equation governing the dynamics in a long wavelength limit.

Starting in real space, the two coupled equations read:

$$(i\partial_t - U^I)p^{I_X}_\mu = -\sum_\kappa \frac{t_{\mu\kappa}}{Z} p^{\bar{I}_{\bar{X}}}_\kappa. \tag{30}$$

Here, the notation $\bar{I}$ and $\bar{X}$ denotes the opposite value of I and X, respectively. Only hole excitations $I = 0$ of spin $\uparrow$ and particle excitations $I = 1$ with spin $\downarrow$ are supported on sublattice A, and vice versa on B. All other ones are trivial and omitted. Therefore, particle excitations on A are tunnel-coupled to hole excitations on B and vice versa. We introduce the effective spinor

$$\psi_{\mu\in A} = \begin{pmatrix} \hat{c}_{\mu\downarrow I=1} \\ \hat{c}_{\mu\uparrow I=0} \end{pmatrix} \quad \psi_{\mu\in B} = \begin{pmatrix} \hat{c}_{\mu\uparrow I=1} \\ \hat{c}_{\mu\downarrow I=0} \end{pmatrix}, \tag{31}$$

which allows us to express the coupled system 30 as:

$$i\partial_t \psi_\mu = \begin{pmatrix} U & 0 \\ 0 & 0 \end{pmatrix} \psi_\mu - \frac{1}{Z} \sum_\kappa t_{\mu\kappa} \sigma_x \psi_\kappa. \tag{32}$$

Applying the trivial phase redefinition $\psi_\mu \to e^{-iUt/2}\psi_\mu$, this becomes:

$$i\partial_t \psi_\mu = \frac{U}{2}\sigma_z \psi_\mu - \frac{1}{Z}\sum_\kappa t_{\mu\kappa}\sigma_x \psi_\kappa \tag{33}$$

with the Pauli matrices σ_x and σ_z. At this point we aim to take the continuum limit, which is appropriate when the quasi-particle wavelength is much larger than the lattice spacing. As a first step, we derive the dispersion relation. Moving to Fourier space we go from the real space hopping element $t_{\mu\nu}$ to the momentum dependent coefficient $t_{\mathbf{k}}$ and find:

$$\omega(\mathbf{k})\psi_{\mathbf{k}} = \left(\frac{U}{2}\sigma_z - t_{\mathbf{k}}\sigma_x\right)\psi_{\mathbf{k}}, \tag{34}$$

which leads to:

$$\omega(\mathbf{k}) = \pm\sqrt{\frac{U^2}{4} + t_{\mathbf{k}}^2}. \tag{35}$$

The minimum gap of the spectrum occurs when $t_{\mathbf{k}_0} = 0$. Expanding $t_{\mathbf{k}}$ around this zero momentum, $\mathbf{k} = \mathbf{k}_0 + \mathbf{q}$ yields:

$$t_{\mathbf{k}}\,\sigma_x\psi_{\mathbf{k}} = \mathbf{q}\cdot\left(\nabla_{\mathbf{k}} t_{\mathbf{k}}\Big|_{\mathbf{k}_0}\right)\sigma_x\psi_{\mathbf{k}} = \mathbf{q}\cdot\mathbf{c}_{\text{eff}}\,\sigma_x\psi_{\mathbf{k}}, \tag{36}$$

where we identify the effective propagation velocity as: $\mathbf{c}_{\text{eff}} = \nabla_{\mathbf{k}} t_{\mathbf{k}}\Big|_{\mathbf{k}_0}$.

Substituting this back, the equation becomes:

$$i\partial_t\psi_{\mathbf{k}} = \left(\frac{U}{2}\sigma_z - \mathbf{c}_{\text{eff}}\cdot\mathbf{q}\,\sigma_x\right)\psi_{\mathbf{k}}. \tag{37}$$

Upon replacing $\mathbf{q} \to -i\nabla$ and Fourier transforming to real space, we arrive at the Dirac equation in 1+1 dimensions with a finite mass term U, separating the upper and lower Hubbard bands.

A parallel calculation for a bipartite semiconductor background leads instead to a Weyl-type equation: the eigenmodes of the two sublattices become coupled, but with zero mass gap. This occurs at momentum $\pi/2$, where both the weakly and strongly correlated layers reach their minimum energy gap.

4.4 | Angle-of-Incidence Dependence

The incident angle φ of the particles can be calculated from the dispersion relation Equation (17) and the parallel momentum $k^{\parallel}$ via

$$\begin{aligned}\varphi &= \arctan\left(\frac{k^{\parallel}}{\kappa_{\text{semi}}}\right)\\ &= \arctan\left(\frac{k^{\parallel}}{\arccos\left[\frac{Z}{2t}(V-E) - \cos k^{\parallel}\right]}\right).\end{aligned} \tag{38}$$

Note that this equation does not yield a solution for any arbitrary triples of energy E, on-site potential V, hopping strength t and parallel momentum κ_{semi}. The angle dependent reflection $R = -\frac{J^{\text{ref}}}{J^{\text{in}}}$ is shown in Figure 5 for three different band alignments. Figure 5a shows the $E > U/2$ case, Figure 5c,d the $E < U/2$ case for $V = 0.4U$ and $V = 0.2U$, respectively.

For $E > U/2$, the minimal reflection is found for energies inside the upper Hubbard band (e.g. $E = 1.01U$) for $\varphi = 0$ and transmission decreases with increasing angle, while for energies below the Hubbard band edge (e.g. $E = 0.96U$ and $E = 0.99U$) minima are found for $\varphi \neq 0$. The relation is reversed, increasing the angle increases transmission, until reflection from the even into the odd spinor turns on, see the kinks in Figure 5b. This shows $-J^{\text{ref}}$, $-J^{\text{ref,sym}}$ and $-J^{\text{ref,asym}}$ for an energy slightly below the upper Hubbard band.

The analogous behavior in the Klein paradox regime, $E < U/2$, can be seen in Figure 5c,d: if the energy for a certain band alignment does not allow for the reflection to be larger than one, it decreases with increasing the angle until reflection into the odd spinor turns on (blue line in Figure 5d). If above-unity reflection is possible, its magnitude increases with increasing the angle.

5 | Conclusions and Outlook

Using the hierarchy of correlations, we investigated a single interface between a weakly interacting layer and a strongly interacting Mott insulator in the Mott–Neel type spin-ordered background. We found an analog to quantum electrodynamics, as in the vicinity of the minimum gap the doublons and holons are effectively described by a Dirac equation. We derived the propagation of the electrons as well as the doublons and holons in their respective regions. For an incoming electron, we calculated the reflection and transmission characteristics, showing that for energies exceeding half the bandgap the system behaves like a potential barrier known from standard quantum mechanics. For energies below, we found behavior reminiscent of the Klein paradox, with reflections greater than one and negative transmission coefficients. This shows that this interface is another condensed matter system that can serve as an analog to the Klein paradox. Some candidates for such interfaces are $SrTiO_3$ substrates with $SmTiO_3$, $LaTiO_3$ or $LaVO_3$ films, characterized by values of $V/U \approx 0.3$ and $V/U \approx 0.55$ [58]. We note that the creation of many doublon–holon pairs in the Klein paradox analog would alter the mean-field background $\hat{\rho}^0$ significantly, such that the back-reaction of this onto the mean-field background, an effect included in the higher-order equation $i\partial_t\hat{\rho}_\mu = F_1(\hat{\rho}_\mu, \hat{\rho}^{\text{corr}}_{\mu\nu})$, should be included in the treatment. This effect is of order $1/Z^2$ or t^2/U^2 and can be neglected in this first approach. Additionally, the heating due to the creation of many pairs might destroy the spin order necessary for the analogy to QED. Therefore, our analysis can describe only the onset of the dielectric breakdown of the Mott insulator. The consequence of a finite pair creation rate is postponed to future work, in which one could use higher order terms of the hierarchy of correlations [59] to calculate Green functions to employ the Meir–Wingreen formalism [60].

Acknowledgements

The authors thank F. Queisser and R. Schützhold for fruitful discussions and valuable feedback on the manuscript. This work is funded by the Deutsche Forschungsgemeinschaft (DFG, German Research Foundation) – Project-ID 278162697– SFB 1242.

Open access funding enabled and organized by Projekt DEAL.

Conflicts of Interest

The author declare no conflicts of interest.

Data Availability Statement

The data that support the findings of this study are available from the corresponding author upon reasonable request.

References

1. O. Klein, "Die Reflexion von Elektronen an einem Potentialsprung Nach der Relativistischen Dynamik Von Dirac," *Zeitschrift für Physik* 53, no. 3 (1929): 157.

2. N. Dombey and A. Calogeracos, "Seventy Years of the Klein Paradox," *Physics Reports* 315, no. 1–3 (1999): 41.

3. A. Hansen and F. Ravndal, "Klein's Paradox and Its Resolution," *Physica Scripta* 23, no. 6 (1981): 1036.

4. J. D. Bjorken and S. D. Drell, "*Sidney David Relativistic Quantum Mechanics*," 1964, McGraw-Hill.

5. W. Greiner, B. Müller, and J. Rafelski, *Quantum Electrodynamics of Strong Fields: With an Introduction into Modern Relativistic Quantum Mechanics* (Springer-Verlag, 1985).

6. C. A. Manogue, "The Klein Paradox and Superradiance," *Annals of Physics* 181, no. 2 (1988): 261.

7. B. R. Holstein, "Klein's Paradox," *American Journal of Physics* 66, no. 6 (1998): 507.

8. H. Nitta, T. Kudo, and H. Minowa, "Motion of a Wave Packet in the Klein Paradox," *American Journal of Physics* 67, no. 11 (1999): 966.

9. M. Merad, L. Chetouani, and A. Bounames, "Boundary Conditions for One-Dimensional Feshbach–Villars Equation," *Physics Letters A* 267, no. 4 (2000): 225.

10. N. Dombey, P. Kennedy, and A. Calogeracos, "Supercriticality and Transmission Resonances in the Dirac Equation," *Physical Review Letters* 85, no. 9 (2000): 1787.

11. P. Krekora, Q. Su, and R. Grobe, "Klein Paradox in Spatial and Temporal Resolution," *Physical Review Letters* 92, no. 4 (2004): 040406.

12. P. Krekora, Q. Su, and R. Grobe, "Klein Paradox with Spin-Resolved Electrons and Positrons," *Physical Review A* 72, no. 6 (2005): 064103.

13. P. Hejcik and T. Cheon, "Anomalous Relativistic Tunneling and Exotic Point Interactions," *Europhysics Letters* 81, no. 5 (2008): 50001.

14. M. I. Katsnelson, K. S. Novoselov, and A. K. Geim, "Chiral Tunnelling and the Klein Paradox in Graphene," *Nature Physics* 2, no. 9 (2006): 620.

15. N. Stander, B. Huard, and D. Goldhaber-Gordon, "Evidence for Klein Tunneling in Graphene P-N Junctions," *Physical Review Letters* 102, no. 2 (2009): 026807.

16. W.-Y. He, Z.-D. Chu, and L. He, "Chiral Tunneling in a Twisted Graphene Bilayer," *Physical Review Letters* 111, no. 6 (2013): 066803.

17. C. Gutiérrez, L. Brown, C.-J. Kim, J. Park, and A. N. Pasupathy, "Klein Tunnelling and Electron Trapping in Nanometre-Scale Graphene Quantum Dots," *Nature Physics* 12, no. 11 (2016): 1069.

18. É. Brézin and C. Itzykson, "Pair Production in Vacuum by an Alternating Field," *Physical Review D* 2, no. 7 (1970): 1191.

19. N. B. Narozhny and A. I. Nikishov, "Pair Production by a Constant External Field," *Soviet Physics JETP* 38, no. 2 (1974): 427.

20. R. Wagner, M. Ware, Q. Su, and R. Grobe, "Bosonic Analog of the Klein Paradox," *Physical Review A* 81, no. 2 (2010): 024101.

21. C. Mayoral, A. Fabbri, and M. Rinaldi, "Steplike Discontinuities in Bose-Einstein Condensates and Hawking Radiation: Dispersion Effects," *Physical Review D* 83, no. 12 (2011): 124047.

22. R. Brito, V. Cardoso, and P. Pani, "Superradiance–the 2020 Edition," *arXiv preprint arXiv:1501.06570* (2015).

23. J. Harms, H. Yuan, and R. A. Duine, "Enhanced Magnon Spin Current Using the Bosonic Klein Paradox," *Physical Review Applied* 18, no. 6 (2022): 064026.

24. E. Kleinherbers, S. P. Kelly, and Y. Tserkovnyak, "Entangling Color Centers via Magnon-Antimagnon Pair Creation," *Physical Review Letters* 134, no. 17 (2025): 176703.

25. A. L. Bassant, M. E. Regout, J. S. Harms, and R. A. Duine, "Entangled Magnon-Pair Generation in a Driven Synthetic Antiferromagnet," *Physical Review B* 110, no. 9 (2024): 094441.

26. A. M. Pineiro, D. Genkina, M. Lu, and I. B. Spielman, "Sauter-Schwinger Effect with a Quantum Gas," *New Journal of Physics* 21 (2019): 083035.

27. D. Witthaut, T. Salger, S. Kling, C. Grossert, and M. Weitz, "Effective Dirac Dynamics of Ultracold Atoms in Bichromatic Optical Lattices," *Physical Review A* 84 (2011): 033601.

28. J. I. Cirac, P. Maraner, and J. K. Pachos, "Cold Atom Simulation of Interacting Relativistic Quantum Field Theories," *Physical Review Letters* 105 (2010): 190403.

29. S.-L. Zhu, B. Wang, and L.-M. Duan, "Simulation and Detection of Dirac Fermions with Cold Atoms in an Optical Lattice," *Physical Review Letters* 98 (2007): 260402.

30. J.-M. Hou, W.-X. Yang, and X.-J. Liu, "Massless Dirac Fermions in a Square Optical Lattice," *Physical Review A* 79 (2009): 043621.

31. L.-K. Lim, C. M. Smith, and A. Hemmerich, "Staggered-Vortex Superfluid of Ultracold Bosons in an Optical Lattice," *Physical Review Letters* 100 (2008): 130402.

32. O. Boada, A. Celi, J. I. Latorre, and M. Lewenstein, "Dirac Equation for Cold Atoms in Artificial Curved Spacetimes," *New Journal of Physics* 13 (2011): 035002.

33. N. Goldman, A. Kubasiak, A. Bermudez, P. Gaspard, M. Lewenstein, and M. A. Martin-Delgado, "Non-Abelian Optical Lattices: Anomalous Quantum Hall Effect and Dirac Fermions," *Physical Review Letters* 103 (2009): 035301.

34. V. Kasper, F. Hebenstreit, M. Oberthaler, and J. Berges, "Schwinger Pair Production with Ultracold Atoms," *Physics Letters B* 760 (2016): 742.

35. F. Queisser, P. Navez, and R. Schützhold, "Sauter-Schwinger-Like Tunneling in Tilted Bose-Hubbard Lattices in the Mott Phase," *Physical Review A* 85 (2012): 033625.

36. N. Szpak and R. Schützhold, "Optical Lattice Quantum Simulator for Quantum Electrodynamics in Strong External Fields: Spontaneous Pair Creation and the Sauter–Schwinger Effect," *New Journal of Physics* 14 (2012): 035001.

37. N. Szpak and R. Schützhold, "Quantum Simulator for the Schwinger Effect with Atoms in Bichromatic Optical Lattices," *Physical Review A* 84 (2011): 050101.

38. M. F. Linder, A. Lorke, and R. Schützhold, "Analog Sauter-Schwinger Effect in Semiconductors for Spacetime-Dependent Fields," *Physical Review B* 97 (2018): 035203.

39. S. A. Smolyansky, A. V. Tarakanov, and M. Bonitz, "Vacuum Particle Creation: Analogy with the Bloch Theory in Solid State Physics," *Contributions to Plasma Physics* 49 (2009): 575.

40. L. Hrivnák, "Relativistic Analogies in Direct-Gap Semiconductors," *Progress in Quantum Electronics* 17 (1993): 235.

41. N. Schopohl and G. E. Volovik, "Schwinger Pair Production in the Orbital Dynamics of ^{3}He-B," *Annals of Physics* 215 (1992): 372.

42. F. Queisser, K. Krutitsky, P. Navez, and R. Schützhold, "Doublon–Holon Pair Creation in Mott–Hubbard Systems in Analogy to QED," *New Journal of Physics* 27, no. 2 (2025): 023030.

43. T. Oka and H. Aoki, "Ground-State Decay Rate for the Zener Breakdown in Band and Mott Insulators," *Physical Review Letters* 95, no. 13 (2005): 137601.

44. T. Oka and H. Aoki, "Dielectric Breakdown in a Mott Insulator: Many-Body Schwinger-Landau-Zener Mechanism Studied with a Generalized Bethe Ansatz," *Physical Review B* 81, no. 3 (2010): 033103.

45. Z. Lenarčič and P. Prelovšek, "Dielectric Breakdown in Spin-Polarized Mott Insulator," *Physical Review Letters* 108, no. 19 (2012): 196401.

46. J. Hubbard, "Electron Correlations in Narrow Energy Bands," *Proceedings of the Royal Society of London, Series A, Mathematical and Physical Sciences* 276, no. 1365 (1963): 238.

47. L. D. Landau, "The Theory of a Fermi Liquid," *Soviet Physics JETP* 3, no. 6 (1957): 920.

48. V. Solovyev and I. Kukushkin, "Renormalized Landau Quasiparticle Dispersion Revealed by Photoluminescence Spectra from a Two-Dimensional Fermi Liquid at the MgZnO/ZnO Heterointerface," *Physical Review B* 96, no. 11 (2017): 115131.

49. F. Queisser, K. V. Krutitsky, P. Navez, and R. Schützhold, "Equilibration and Prethermalization in the Bose-Hubbard and Fermi-Hubbard Models," *Physical Review A* 89 (2014): 033616.

50. F. Queisser and R. Schützhold, "Environment-Induced Prerelaxation in the Mott-Hubbard Model," *Physical Review B* 99, no. 15 (2019): 155110.

51. P. Navez and R. Schützhold, "Emergence of Coherence in the Mott-Insulator–Superfluid Quench of the Bose-Hubbard Model," *Physical Review A* 82 (2010): 063603.

52. J. Verlage and P. Kratzer, "Bound States at Semiconductor–Mott Insulator Interfaces," *Physical Review B* 113 (2026): 045110.

53. J. Hubbard, "Electron Correlations in Narrow Energy Bands-IV. The Atomic Representation," *Proceedings of the Royal Society of London, Series A, Mathematical and Physical Sciences* 285, no. 1403 (1965): 542.

54. S. G. Ovchinnikov and V. V. Val'kov, *Hubbard Operators in the Theory of Strongly Correlated Electrons* (World Scientific, 2004).

55. F. Mancini and A. Avella, "The Hubbard Model Within the Equations of Motion Approach," *Advances in Physics* 53, no. 5-6 (2004): 537.

56. J. Verlage, F. Queisser, N. Szpak, J. König, P. Kratzer, and R. Schützhold, "Quasi-Particle Propagation Across Semiconductor–Mott Insulator Interfaces," *International Journal of Theoretical Physics* 63, no. 11 (2024): 1.

57. P. Navez, F. Queisser, and R. Schützhold, "Quasi-Particle Approach for Lattice Hamiltonians with Large Coordination Numbers," *Journal of Physics A: Mathematical and Theoretical* 47, no. 22 (2014): 225004.

58. L. Bjaalie, A. Azcatl, S. McDonnell, C. R. Freeze, S. Stemmer, et al., "Band Alignments Between $SmTiO_3$, $GdTiO_3$, and $SrTiO_3$," *Journal of Vacuum Science and Technology A* 34, no. 6 (2016): 061102.

59. F. Queisser, C. Kohlfürst, and R. Schützhold, "Back-Reaction and Correlation Effects on Prethermalization in Mott-Hubbard Systems," *Physical Review B* 109 (2024): 195140.

60. Y. Meir and N. S. Wingreen, "Landauer Formula for the Current Through an Interacting Electron Region," *Physical Review Letters* 68 (1992): 2512.

61. F. Queisser and R. Schützhold, "Hierarchy of Double-Time Correlations," *Journal of Statistical Mechanics: Theory and Experiment* 2023, no. 5 (2023): 053101.

62. I. Avigo, F. Queisser, P. Zhou, M. Ligges, K. Rossnagel, et al., "Doublon Bottleneck in the Ultrafast Relaxation Dynamics of Hot Electrons in $1T\!-\!TaS_2$," *Physical Review Research* 2 (2020): 022046.

Appendix A: Hierarchy of Correlations

In order to describe the (quasi-)particles in the heterostructure, we employ the *hierarchy of correlations* approach [49–51]. This method starts from a general lattice Hamiltonian of the form:

$$\hat{H} = \frac{1}{Z}\sum_{\mu\nu}\hat{H}_{\mu\nu} + \sum_{\mu}\hat{H}_{\mu}, \tag{A1}$$

where μ and ν are generalized lattice coordinates and Z is the coordination number. In the regime of large coordination number $Z \gg 1$, a controlled truncation scheme becomes possible, yielding a closed and iterative set of equations.

The approach begins with the Heisenberg equation of motion for the density operator $\hat{\rho}$:

$$i\partial_t\hat{\rho} = [\hat{H},\hat{\rho}] = \frac{1}{Z}\sum_{\mu\nu}\hat{\mathcal{L}}_{\mu\nu}\hat{\rho} + \sum_{\mu}\hat{\mathcal{L}}_{\mu}\hat{\rho}, \tag{A2}$$

where the Liouville superoperators are defined as $\hat{\mathcal{L}}_{\mu\nu}(\hat{\rho}) = [\hat{H}_{\mu\nu},\hat{\rho}]$ and $\hat{\mathcal{L}}_{\mu}(\hat{\rho}) = [\hat{H}_{\mu},\hat{\rho}]$.

Since physical observables are typically defined over a subset of lattice sites, we decompose the reduced density matrices into uncorrelated and correlated parts:

$$\begin{aligned}\hat{\rho}_{\mu\nu} &= \hat{\rho}^{\text{corr}}_{\mu\nu} + \hat{\rho}_{\mu}\hat{\rho}_{\nu},\\ \hat{\rho}_{\mu\nu\lambda} &= \hat{\rho}^{\text{corr}}_{\mu\nu\lambda} + \hat{\rho}^{\text{corr}}_{\mu\nu}\hat{\rho}_{\lambda} + \hat{\rho}^{\text{corr}}_{\mu\lambda}\hat{\rho}_{\nu} + \hat{\rho}^{\text{corr}}_{\nu\lambda}\hat{\rho}_{\mu} + \hat{\rho}_{\mu}\hat{\rho}_{\nu}\hat{\rho}_{\lambda},\end{aligned} \tag{A3}$$

and so on for higher-order correlations.

The time evolution of the on-site density operator $\hat{\rho}_{\mu}$ is given by:

$$i\partial_t\hat{\rho}_{\mu} = \frac{1}{Z}\sum_{\alpha\neq\mu}\text{tr}_{\alpha}\left(\hat{\mathcal{L}}^{S}_{\alpha\mu}\left[\hat{\rho}^{\text{corr}}_{\mu\alpha} + \hat{\rho}_{\alpha}\hat{\rho}_{\mu}\right]\right) + \hat{\mathcal{L}}_{\mu}\hat{\rho}_{\mu}, \tag{A4}$$

where the symmetrized Liouvillian is $\hat{\mathcal{L}}^{S}_{\mu\nu} = \hat{\mathcal{L}}_{\mu\nu} + \hat{\mathcal{L}}_{\nu\mu}$. This equation couples to the two-point correlator $\hat{\rho}^{\text{corr}}_{\mu\nu}$.

A similar procedure applies to the evolution of $\hat{\rho}^{\text{corr}}_{\mu\nu}$, resulting in:

$$\begin{aligned} i\partial_t\hat{\rho}^{\text{corr}}_{\mu\nu} = {}& \hat{\mathcal{L}}_{\mu}\hat{\rho}^{\text{corr}}_{\mu\nu} + \frac{1}{Z}\hat{\mathcal{L}}_{\mu\nu}\left(\hat{\rho}^{\text{corr}}_{\mu\nu} + \hat{\rho}_{\mu}\hat{\rho}_{\nu}\right)\\ & - \frac{\hat{\rho}_{\mu}}{Z}\,\text{tr}_{\mu}\left(\hat{\mathcal{L}}^{S}_{\mu\nu}\left[\hat{\rho}^{\text{corr}}_{\mu\nu} + \hat{\rho}_{\mu}\hat{\rho}_{\nu}\right]\right)\\ & + \frac{1}{Z}\sum_{\alpha\neq\mu,\nu}\text{tr}_{\alpha}\left(\hat{\mathcal{L}}^{S}_{\mu\alpha}\left[\hat{\rho}^{\text{corr}}_{\mu\nu\alpha} + \hat{\rho}^{\text{corr}}_{\mu\nu}\hat{\rho}_{\alpha} + \hat{\rho}^{\text{corr}}_{\nu\alpha}\hat{\rho}_{\mu}\right]\right)\\ & + (\mu\leftrightarrow\nu).\end{aligned} \tag{A5}$$

This equation introduces the three-point correlator $\hat{\rho}^{\text{corr}}_{\mu\nu\lambda}$, and so the equations form an infinite hierarchy:

$$\begin{aligned} i\partial_t\hat{\rho}_{\mu} &= F_1(\hat{\rho}_{\mu},\hat{\rho}^{\text{corr}}_{\mu\nu}),\\ i\partial_t\hat{\rho}^{\text{corr}}_{\mu\nu} &= F_2(\hat{\rho}_{\mu},\hat{\rho}^{\text{corr}}_{\mu\nu},\hat{\rho}^{\text{corr}}_{\mu\nu\lambda}),\\ i\partial_t\hat{\rho}^{\text{corr}}_{\mu\nu\lambda} &= F_3(\hat{\rho}_{\mu},\hat{\rho}^{\text{corr}}_{\mu\nu},\hat{\rho}^{\text{corr}}_{\mu\nu\lambda},\hat{\rho}^{\text{corr}}_{\mu\nu\lambda\kappa}),\\ i\partial_t\hat{\rho}^{\text{corr}}_{\mu\nu\lambda\alpha} &= F_4(\hat{\rho}_{\mu},\hat{\rho}^{\text{corr}}_{\mu\nu},\hat{\rho}^{\text{corr}}_{\mu\nu\lambda},\hat{\rho}^{\text{corr}}_{\mu\nu\lambda\kappa},\hat{\rho}^{\text{corr}}_{\mu\nu\lambda\kappa\beta}).\end{aligned} \tag{A6}$$

The exact form of the functionals F_n depends on the specific structure of the Hamiltonian.

If the initial state exhibits a scaling behavior where ℓ-point correlations scale as $\mathcal{O}(Z^{-\ell+1})$, this property is preserved throughout time evolution [49, 61]. This scaling allows for a systematic truncation of the hierarchy. Keeping only the leading orders yields:

$$\begin{aligned} i\partial_t\hat{\rho}_{\mu} &\approx F_1(\hat{\rho}_{\mu},0), \quad \text{with solution } \hat{\rho}^{0}_{\mu},\\ i\partial_t\hat{\rho}^{\text{corr}}_{\mu\nu} &\approx F_2(\hat{\rho}^{0}_{\mu},\hat{\rho}^{\text{corr}}_{\mu\nu},0).\end{aligned} \tag{A7}$$

These two equations form the basis for describing the charge modes in the heterostructure. The quantity $\hat{\rho}^0_\mu$ captures the mean-field background, encoding the charge and spin structure of the system.

Appendix B: Hierarchy for the Fermi Hubbard Model

To apply the hierarchy of correlations to the Fermi–Hubbard model defined in Equation (1), we begin by introducing the spin background. This is represented by the antiferromagnetic Mott–Néel state, in which the lattice is divided into two sublattices, A and B, arranged in a checkerboard configuration:

$$\hat{\rho}^0_\mu = \begin{cases} |\uparrow\rangle_\mu \langle \uparrow| & \mu \in A, \\ |\downarrow\rangle_\mu \langle \downarrow| & \mu \in B. \end{cases} \tag{B1}$$

Irrespective of the choice of mean-field background, it is useful to define quasi-particle operators. These are inspired by the Hubbard X-operators [53, 54] and composite operator approaches [55], and are written as:

$$\hat{c}_{\mu s I} = \hat{c}_{\mu s} \hat{n}^I_{\mu \bar{s}} = \begin{cases} \hat{c}_{\mu s}(1 - \hat{n}_{\mu \bar{s}}) & \text{for } I = 0, \\ \hat{c}_{\mu s} \hat{n}_{\mu \bar{s}} & \text{for } I = 1, \end{cases} \tag{B2}$$

where $I = 0$ and $I = 1$ label holons and doublons, respectively. These operators offer a more accurate description of the relevant physical processes, although they only approximate the actual quasi-particle creation and annihilation operators for holons and doublons [62]. Here, $\bar{s}$ denotes the spin opposite to s.

We now consider the two-point correlation functions $\langle \hat{c}^\dagger_{\mu s I} \hat{c}_{\nu s J} \rangle$, whose time evolution is given by:

$$\begin{aligned} i\partial_t \langle \hat{c}^\dagger_{\mu s I} \hat{c}_{\nu s J} \rangle^{\text{corr}} &= \frac{1}{Z} \sum_{\lambda L} t_{\mu\lambda} \langle \hat{n}^I_{\mu \bar{s}} \rangle^0 \langle \hat{c}^\dagger_{\lambda s L} \hat{c}_{\nu s J} \rangle^{\text{corr}} \\ &\quad - \frac{1}{Z} \sum_{\lambda L} t_{\nu\lambda} \langle \hat{n}^J_{\nu \bar{s}} \rangle^0 \langle \hat{c}^\dagger_{\mu s I} \hat{c}_{\lambda s L} \rangle^{\text{corr}} \\ &\quad + \left(U^J_\nu - U^I_\mu + V_\nu - V_\mu \right) \langle \hat{c}^\dagger_{\mu s I} \hat{c}_{\nu s J} \rangle^{\text{corr}} \\ &\quad + \frac{t_{\mu\nu}}{Z} \left(\langle \hat{n}^I_{\mu \bar{s}} \rangle^0 \langle \hat{n}^1_{\nu s} \hat{n}^J_{\nu \bar{s}} \rangle^0 - \langle \hat{n}^J_{\nu \bar{s}} \rangle^0 \langle \hat{n}^1_{\mu s} \hat{n}^I_{\mu \bar{s}} \rangle^0 \right) \\ &\quad + \mathcal{O}(1/Z^2), \end{aligned} \tag{B3}$$

where we define $U^I_\mu = I U_\mu$, so that $U^I_\mu = 0$ for $I = 0$ and $U^I_\mu = U_\mu$ for $I = 1$.

The dynamical evolution of these correlations can be further simplified using a factorization approach [49, 57], allowing us to isolate the amplitudes for holons ($I, J = 0$) and doublons ($I, J = 1$).

In the bipartite lattice structure, each sublattice has a distinct spin occupation: sites on sublattice X satisfy $\langle \hat{n}_{\mu_X \uparrow} \rangle = 0$ and $\langle \hat{n}_{\mu_X \downarrow} \rangle = 1$, while the opposite holds for sites on sublattice Y. The correlation functions can be expressed in terms of Fourier components with an additional index to distinguish sublattices:

$$\langle \hat{c}^\dagger_{\mu_X s I} \hat{c}_{\nu_Y s J} \rangle^{\text{corr}} = \left(p^{I_X}_{\mu s} \right)^* p^{J_Y}_{\nu s}, \tag{B4}$$

where $X, Y \in \{A, B\}$ refer to the sublattices. These amplitudes can be conveniently grouped using a spinor notation, and their dynamics are governed by effective equations [56].

Assuming a highly symmetric (e.g., hypercubic) lattice permits a Fourier transform along the directions parallel to the interface:

$$\begin{aligned} p^{I_X}_{\mu s} &= \frac{1}{\sqrt{N^\parallel}} \sum_{\mathbf{k}^\parallel} p^{I_X}_{n, \mathbf{k}^\parallel, s} e^{i \mathbf{k}^\parallel \cdot \mathbf{x}^\parallel_\mu}, \\ t_{\mu\nu} &= \frac{Z}{N^\parallel} \sum_{\mathbf{k}^\parallel} t_{m,n,\mathbf{k}^\parallel} e^{i \mathbf{k}^\parallel \cdot \left(\mathbf{x}^\parallel_\mu - \mathbf{x}^\parallel_\nu \right)}. \end{aligned} \tag{B5}$$

For isotropic nearest-neighbor hopping with $t^\parallel_n = t^\perp_{n,n-1} = t$, the hopping matrix elements take the form:

$$\begin{aligned} t_{m,n,\mathbf{k}^\parallel} &= \frac{t^\parallel_{\mathbf{k}^\parallel}}{Z} \delta_{m,n} + \frac{t}{Z} (\delta_{n,n-1} + \delta_{n,n+1}), \\ t^\parallel_{\mathbf{k}^\parallel} &= 2t \sum_{x_i} \cos(p^\parallel_{x_i}) \equiv Z t^\parallel_{\mathbf{k}}, \end{aligned} \tag{B6}$$

where $t^\parallel_{\mathbf{k}}$ captures the momentum-dependent in-plane hopping.

The resulting doublon and holon amplitudes obey the coupled equations:

$$\left(i\partial_t - U^j \right) p^{I_X}_{\mu s} = -\langle \hat{n}^I_{\mu_X} \rangle \sum_L \left[t^\parallel_{\mathbf{k}} p^{L_{\bar{X}}}_\mu + \frac{t}{Z} \left(p^{L_{\bar{X}}}_{\mu+1} + p^{L_{\bar{X}}}_{\mu-1} \right) \right], \tag{B7}$$

where $\bar{X}$ denotes the sublattice opposite to X.

Finally, assuming without loss of generality that $\langle \hat{n}_{\mu_A \uparrow} \rangle = 0$ and $\langle \hat{n}_{\mu_B \downarrow} \rangle = 0$, it follows directly that

$$E\, p^{1_A}_\mu = (E - U)\, p^{0_B}_\mu \equiv 0.$$